CORA Cork Open Research Archive
Cartlann Taighde Oscailte Chorcaí

Title	3-D printed surface-mounted ceramic filters: temperature drift effect on coupling parameters
Authors	Fontana, Andrés;Périgaud, Aurélien;Delhote, Nicolas;Richard, Patrice;Carsenat, David;Acikalin, Guillaume
Publication date	2024-03-27
Original Citation	Fontana, A., Périgaud, A., Delhote, N., Richard, P., Carsenat, D. and Acikalin, G. (2024) '3-D printed surface-mounted ceramic filters: temperature drift effect on coupling parameters', 2024 IEEE International Microwave Filter Workshop (IMFW), Cocoa Beach, FL, USA, 21-23 February 2024, pp. 112-114. https://doi.org/10.1109/IMFW59690.2024.10477156
Type of publication	Conference item;proceedings-article
Link to publisher's version	10.1109/imfw59690.2024.10477156
Rights	© 2024, IEEE. Personal use of this material is permitted. Permission from IEEE must be obtained for all other uses, in any current or future media, including reprinting/republishing this material for advertising or promotional purposes, creating new collective works, for resale or redistribution to servers or lists, or reuse of any copyrighted component of this work in other works.
Download date	2026-11-02 01:32:25
Item downloaded from	https://hdl.handle.net/10468/18020

UCC
University College Cork, Ireland
Coláiste na hOllscoile Corcaigh

3-D Printed Surface-Mounted Ceramic Filters: Temperature Drift Effect on Coupling Parameters

Andrés Fontana
Tyndall National Institute
University College Cork
Cork, Ireland
andres.fontana@tyndall.ie

Aurélien Périgaud
Xlim research institute
CNRS/University of Limoges
Limoges, France
aurelien.perigaud@xlim.fr

Nicolas Delhote
Xlim research institute
CNRS/University of Limoges
Limoges, France
nicolas.delhote@xlim.fr

Patrice Richard
Thales SIX GTS
Brive-la-Gaillarde, France
patrice.richard@thalesgroup.com

David Carsenat
Thales SIX GTS
Brive-la-Gaillarde, France
david.carsenat@thalesgroup.com

Guillaume Acikalin
Thales SIX GTS
Brive-la-Gaillarde, France
guillaume.acikalin@thalesgroup.com

***Abstract*—This study investigates the impact of temperature on four 3D-printed Alumina bandpass filters. Thermal cycling tests from 23 to 80°C reveal a frequency shift of -766 to -554 kHz/°C, depending on the design. The spatial arrangement of coupling iris structures relative to the heat source affects the inter-resonator coupling factors and the bandwidth drift. The results show bandwidth variations of 42 to 55 kHz/°C and insertion loss changes from 0.004 to 0.006 dB/°C.**

***Index Terms*—3-D printed, Alumina, thermal cycling, coupling matrix**

I. Introduction

In recent years, additive manufacturing has significantly advanced 3D-printed microwave filters, exploring materials like metal [1], polymer [2], and ceramics such as Alumina [3]–[5] and Zirconia [6] owing to their high permittivity and low loss properties. The versatility of 3D printing is valuable for developing tuneable strategies [6] and passive filter configurations [4], [7]. Nevertheless, manufacturing tolerances remain a challenge, often requiring post-fabrication tuning methods like tuning screws [3], [4], [6], dielectric tuners [7], and laser ablation corrections [8]. Integrating 3D-printed microwave devices is advantageous in spatially constrained environments, such as aerospace applications. However, challenges like temperature fluctuations must be considered in design to ensure radio system reliability in harsh conditions. Numerous studies have explored temperature effects on microwave devices, with a focus on how thermal expansion and the temperature coefficient of permittivity influence center frequency. This study investigates four surface-mounted 3D-printed ceramic filters introduced in a previous work. The primary objective is to assess how each filter's frequency response deviates in response to a heat source. Additionally, the study aims to confirm the filters' proper functionality through multiple temperature cycles, ranging from room temperature to 80 °C.

This project was co-funded by Thales Six GTS and the region Nouvelle Aquitaine in the frame of the Désirh-3D project.

A. 3-D printed Alumina filters

In [8], a set four surface-mounted ceramic-filled cavity filter arrangements (fig. 1) were introduced to overcome the limitations of 3-D manufacturing. These devices were conceived to provide diverse RF functionalities in wireless transceivers by exploiting the flexibility of ceramic Stereolithography techniques. The prototypes were silver plated and devised to be surface mounted onto a 0.4mm-thick Rogers 4003C board using classical pick and place equipment and a temperature-controlled oven [5]. The in-line 4-pole filters in fig. 1 were designed to meet the same specifications at X-band. Due to the manufacturing tolerances and structural irregularities observed in the bandpass filter samples, denoted as C-shaped (Cs), Bridge, Box, and U-shaped (Us) filters, a post-fabrication laser tuning process was employed on the metal plate. This process was implemented to correct the frequency response deviations and recover the initial specifications.

B. Temperature characterization setup

An experimental temperature analysis was performed to assess the robustness of the printed filters and their response to temperature fluctuations. The implemented setup shown in fig. 2.a comprised a Microtech RF probe station with GSG

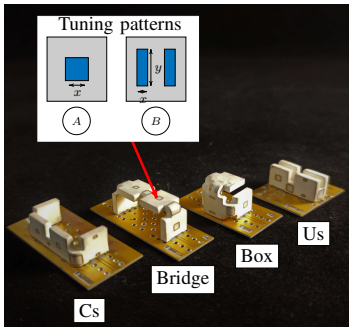


Fig. 1. Surface-mounted laser-tuned 3-D printed filters from left to right: C-shape (Cs), Bridge, Box and U-shape (Us) filters from [8].

0.5 mm probe tip connected to a Rhode & Schwartz ZVA 87 VNA. The devices under test (DUTs) were placed on a Peltier cell controlled by means of a temperature controller. A temperature sensor was positioned on top of the devices (fig. 2.b) and connected to a digital multimeter to monitor the temperature difference between the PCB and the DUT. The thermal cycles were set between ambient temperature and 80 °C following a smooth temperature profile to allow the heat to be homogeneously distributed in the sample. However, a different frequency behavior was expected in every design owing to the significant thermal conductivity (better than 25 W/m.K) of Alumina.

II. Measured Results During Thermal Cycling

The DUTs were exposed individually to three sequential temperature cycles: 1) heating stage from room temperature ($T_{min} = 23\ °C$) up to $T_{max} = 80\ °C$ (maximum temperature supported by the Peltier cell) in steps from temperature T1 to T2 of $\Delta T = T_2 - T_1 = 5°C$ (insight in fig. 2.a); 2) cooling from T_{max} to T_{min} in steps of $\Delta T = -5°C$, finalizing the cycle; and 3) repeating the whole process two more times. The maximum settling time Δt_s monitored on the samples by the sensor between two temperature steps was less than 3 minutes in every case. The error band established to define the settling time was $e_s = \pm 0.1°C$ (insight in fig. 2.a). While in most cases the Peltier cell and the temperature sensor typically showed a slight temperature difference as the DUTs were heated, the Bridge filter exhibited a more pronounced effect. This phenomenon could result from the non-uniform temperature distribution within the structure due to heat transfer from the carrier board to the input/output resonators. The larger surface area of the Bridge filter in contact with the ambient air may favor the heat dissipation more effectively than the other arrangements. The thermal characterization of this device during the experiment was limited up to $60°C$ to avoid damaging the Peltier cell as a consequence of the temperature difference observed. By contrast, the C- and U-shaped filters are completely soldered to the PCB surface, resulting in a homogeneous heat distribution across the entire sample. The Box filter exhibits an intermediate case in between the C-/U-shaped and Bridge filters. Figure 3 shows the U-shape and Box filter scattering parameters measured at several temperatures. Although the plot exhibits a frequency shift $\Delta fo(T) \simeq fo(T) - fo(23°C)$, the overall filter profile

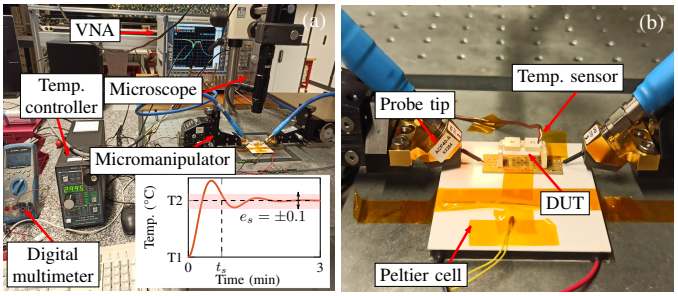


Fig. 2. 3-D printed filters temperature characterization setup (a) and probe tips and sensing elements (b).

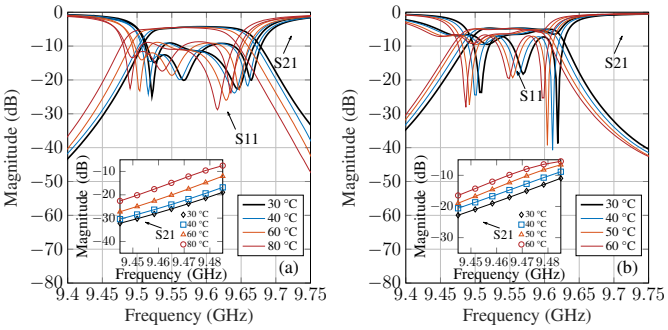


Fig. 3. U-shaped filter (a) and Box filter (b) measured S-parameters between 30 and 80°C.

maintains a similar shape with a slight compression of the pass band $\Delta BW(T) = BW(T) - BW(23°C)$ around a few MHz in both cases. Alumina substrates usually have a negative thermal coefficient of frequency τ_f, typically around -60 ppm/°C. This, combined with device expansion, can cause a frequency shift $\Delta fo(T)$ towards lower values. The data analyzed during a complete thermal cycle shows a linear progression with temperature, driving to a linear fitting of Δf_o (fig. 4.a), ΔBW (fig. 4.b) and the insertion losses (fig. 4.c). The maximum relative center frequency shift observed in fig. 4.a for temperatures up to $80°C$ is between $-42\ MHz \leq \Delta fo(T) \leq -29\ MHz$. The linear regression slope obtained falls within $-766\ kHz/°C \leq \frac{\delta fo}{\delta T} \leq -554\ kHz/°C$, with the Box filter displaying the lowest sensitivity and the Bridge filter exhibiting the highest sensitivity. The temperature-dependent center frequency behavior closely resembles each other for the U- and C-shaped filters, with slopes of $\frac{\delta fo}{\delta T}(Us) \approx -637\ kHz/°C$ and $\frac{\delta fo}{\delta T}(Cs) \approx -629\ kHz/°C$, respectively. While the collective filter response lacks full insight into temperature's impact on individual parameters, coupling matrix factors were extracted from the thermal cycling experiment results to gain a deeper understanding of parameter changes within each filter. Fig. 5.a shows the difference between the extracted main diagonal factors of the coupling matrix and the measured filter at room temperature taken as reference ($\Delta m_{ii}(T) = m_{ii}(T) - m_{ii}(23°C)$). The picture shows the linear evolution of $m_{ii}(T)$ with $i = 1\ to\ 4$ for all the resonators of the different DUTs. It should be noted that in

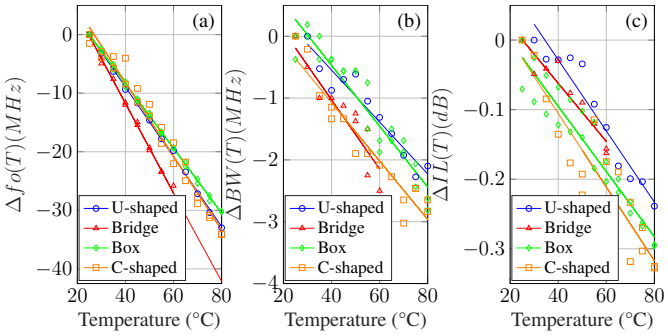


Fig. 4. Additively manufactured ceramic filters response evolution with temperature in one cycle: relative frequency shift (a), relative bandwidth variation (b) and relative increment of losses (c).

the case of the Box and Bridge filters, the separation between the resonators spreads as the temperature increases, whilst in the case of the C- and U-Shaped filters this separation seems to be constant. Concerning the bandwidth variation (fig. 4.b), the filters seem to be divided into two groups: the C-shaped and U-shaped on the one side the Box and Bridge filters and on the other side. These designs show a similar behaviour that could be related to the device heating. In the first group, the coupling irises and resonators come into direct contact with the carrier board. In contrast, in the second group, some of the irises and resonators are not mounted onto the PCB, and consequently, they do not experience direct heating. The relative bandwidth fluctuation with temperature calculated is $\frac{\delta \Delta BW}{\delta T} = -0.042\ MHz/°C$ for the C-shaped and $\frac{\delta \Delta BW}{\delta T} = -0.047\ MHz/°C$ for the U-shaped filter. In the second case these variations are $\frac{\delta \Delta BW}{\delta T} = -0.049\ MHz/°C$ for the Box and $\frac{\delta \Delta BW}{\delta T} = -0.055\ MHz/°C$ for the Bridge filter. The consecutive inter-resonator couplings m_{ij} with $i = 1, 2, 3$ and $j = 2, 3, 4$ illustrated in fig. 5.b to e exhibit also the same tendency between the C-shaped and U-shaped on one side, and between the Bridge and Box filter. As it can be seen, in the first case the coupling factors are more affected by temperature fluctuations, while in the second case they are less dispersed. Furthermore, the coupling factor m_{23} that corresponds to the iris between resonator 2 and 3 shows a lower variation in the last case. This part of the structure seems to be the coldest area within the DUTs. The same observations may be applied to the added losses within the pass band in fig. 4.c, where the behavior of the filters can be subdivided into the same two groups. The highest losses (up to $\Delta IL = IL(T) - IL(23°C) = 0.3\ dB$) were identified in the C-shaped filter. Based on the experimental results, the calculated loss rate with temperature expected for these devices is $0.004\ dB/°C \leq \frac{\delta IL}{\delta T} \leq 0.006\ dB/°C$. The losses increasing are attributed to the metallization conductivity degradation as well as the degradation of the dielectric loss tangent when the ceramic temperature rises.

III. Conclusions

The thermal analysis of 3D-printed filters reveals how temperature variations affect their performance. Depending on their arrangement, individual resonators exhibit varying frequency responses, leading to non-uniform filter pole shifts with increasing temperature. This phenomenon poses a particular concern for narrowband filters, where C-/U-shaped designs demonstrate more consistent frequency shifts due to their evenly distributed heat pattern on the carrier board. In contrast, Box and Bridge configurations show localized heat regions (board contact) and quicker heat dissipation. Regarding frequency response specifications, the filters exhibit satisfactory performance up to 80°C, maintaining their filtering characteristics. They experience a maximum center frequency shift of $\Delta fo(80\ °C) = -42\ MHz$, a bandwidth reduction of $\Delta BW(80\ °C) = -3.135\ MHz$, and extra losses $\Delta IL(80°C) \approx 0.3\ dB$, in the worst-case scenario. No structural damage or significant frequency response degradation was observed during temperature cycling. Future tests will involve subjecting the filters to numerous humidity and temperature cycles in a climatic chamber to complete reliability assessments. Additionally, integrating temperature-stable ceramics into the additive manufacturing process can mitigate temperature influence and enhance stability, catering to more stringent specifications.

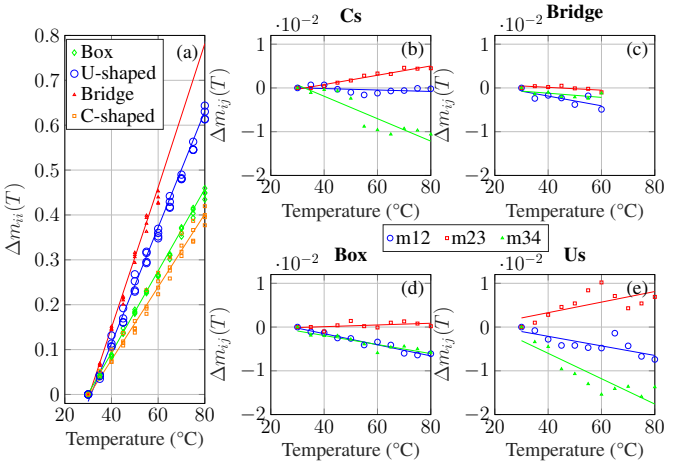


Fig. 5. Normalized coupling matrix factors dependency with temperature extracted from DUTs measurements: main diagonal factors mii (a) and inter-resonator coupling factors mij for the C-shaped (b), Bridge (c), Box (d) and U-shaped (e) filters.

References

[1] O. A. Peverini, M. Lumia, G. Addamo, G. Virone, and N. J. G. Fonseca, "How 3d-printing is changing rf front-end design for space applications," *IEEE Journal of Microwaves*, vol. 3, no. 2, pp. 800–814, 2023.

[2] J. L. Medrán Del Río, A. Fernandez-Prieto, J. Martel, and D. Psychogiou, "Monolithic compact low-frequency bandpass filter based on intertwined helical resonators," in *2023 IEEE/MTT-S International Microwave Symposium - IMS 2023*, 2023, pp. 748–751.

[3] L. Robins, C. Bartlett, A. Arsanjani, A. Widaa, R. Teschl, M. Höft, and W. Bösch, "3d-printed dielectric resonators for quasi-te112 mode singlets, doublets and dual-mode filters," *IEEE Access*, vol. 10, pp. 130 326–130 338, 2022.

[4] P. Vallerotonda, F. Cacciamani, L. Pelliccia, C. Tomassoni, G. Cannone, and V. T. di Crestvolant, "Compact ultra-wideband cavity filter based on suspended ceramic resonators in additive manufacturing," in *2022 IEEE/MTT-S International Microwave Symposium - IMS 2022*, 2022, pp. 92–95.

[5] F. Aquino, D. Tiradossi, L. Pelliccia, A. De Padova, F. Vitulli, S. Di Nardo, and F. Deborgies, "Ka-band cavity filter manufactured in 3d-printed alumina technology," in *2022 52nd European Microwave Conference (EuMC)*, 2022, pp. 123–126.

[6] A. Périgaud, O. Tantot, N. Delhote, S. Verdeyme, S. Bila, D. Pacaud, L. Carpentier, J. Puech, L. Lapierre, and G. Carayon, "Continuously tuned ku-band cavity filter based on dielectric perturbers made by ceramic additive manufacturing for space applications," *Proceedings of the IEEE*, vol. 105, no. 4, pp. 677–687, 2017.

[7] E. López-Oliver, C. Tomassoni, F. Cacciamani, L. Pelliccia, and V. T. D. Crestvolant, "Bandpass filter based on 3-d-printed ceramic resonators," in *2022 24th International Microwave and Radar Conference (MIKON)*, 2022, pp. 1–5.

[8] A. Fontana, A. Delage, A. Périgaud, P. Richard, D. Carsenat, G. Acikalin, S. Verdeyme, B. Bonnet, L. Carpentier, and N. Delhote, "A novel approach toward the integration of fully 3-d printed surface-mounted microwave ceramic filters," *IEEE Transactions on Microwave Theory and Techniques*, vol. 71, no. 9, pp. 3915–3928, 2023.